

Lasers in Manufacturing Conference 2021

Active mirrors for plane field correction in laser material processing

Paul Böttner^{a,*}, Claudia Reinlein^c, Aoife Brady^a, Ramona Eberhardt^a, Stefan Nolte^{a,b}

^a Fraunhofer Institute for Applied Optics and Precision Engineering IOF Albert-Einstein-Straße 7, 07745 Jena, Germany

^b Friedrich-Schiller-Universität Jena, Institute of Applied Physics, Jena, Germany

^c RobustAO GmbH, Jena, Germany

Abstract

This paper reports on an approach to increase the scan field and the dynamic range of post objective scanners. An active mirror in combination with a fixed focusing lens is used to adjust the optimal focus length depending on the beam position in the scan field. The active mirror has an adjustment range of 0.52 dpt with a step response time of 2 ms. The scan field is determined by the focal length of the focusing lens. A permissible spot eccentricity of 0.4 and a focal length of 250 mm enable a work field of (186x140) mm². Doubling the focal length increases the scan field to (420x372) mm². Simulations with a raw beam diameter of 10 mm and a wavelength of 633 nm provide a spot diameter of 29.5 μm with a focal length of 250 mm and 57.4 μm with a focal length of 500 mm.

Keywords: active mirror; material processing, plane field correction, post -objective scanning

1. Introduction

Post-objective scanning based on an active mirror provides a new approach plane field correction that promises more compact and wavelength-independent systems. Conventional post-objective scanning solutions consist of a combination of lens slider and galvanometer scanner. The galvanometer scanner is used to scan the X-Y work plane and consists of two mirrors orthogonal to each other, which allows the laser beam to be guided freely in the X-Y plane. The focus is adjusted by a lens slider placed before the galvanometer in the beam path.

This work replaces the lens slider with an active mirror in combination with a fixed focal lens. An active mirror has the capability to adapt the surface in response to an electrical signal. Thus, by applying an electrical voltage, the active mirror can change its optical power. This allows the focus adjustment and the correction of spot distortions (errors) at large deflection angles of the scan mirrors.

* Corresponding author.

E-mail address: paul.boettner@iof.fraunhofer.de .

Another option for correcting spot distortion in scanner applications is offered by pre-objective scanning. The principle of pre-objective scanning uses an F-theta lens between the galvanometer and the work plane which corrects the spot distortions. The advantage of pre-objective scanning is that, apart from the X-Y mirrors of the galvanometer, no moving parts are necessary.

As discussed in literature the differences of post- and pre-objective scanning become apparent. Pre-objective scanning solutions require increasingly larger optics for larger working fields, while the translational system of post-objective scanning can generate the spot correction with the help of preset configuration parameters (Pelsue, Kurt, 1982, Zaeh et. Al 2010). The dynamic range of pre-objective scanners is determined by the velocity of the X-Y-scanner while in post-objective scanning the translational lens slider determines the velocity for the focus adjustment. Furthermore, lenses are only suitable for high-power laser systems to a limited extent due to the low laser-induced damage thresholds (LIDT) of the coating (Eberle et. al 2013, Wood et.al 2003). Furthermore, the integration of additional wavelengths for sensor and monitoring beam paths turns out to be cumbersome in refractive systems.

Active mirrors have been evaluated repeatedly to offer highly dynamic means of correction and high-power capability (Bayanna, et. al 2015, Kopf et. Al 2017, Reinlein et. Al 2013, S. Verpoort et. Al, 2020, C. Reinlein et. Al, 2021). Therefore, by using an active mirror as a correction element, a large working field in the X-Y plane can be combined with a highly dynamic spot correction and a high laser power. However, an optical analysis of possible scan field sizes and scan speeds in active mirrors in post-objective scanning applications remains open. This work presents a concept of post-objective scanning by implementing an active mirror as a 90° deflection mirror in a collimated beam path. Simulation and experimental measurements demonstrate that the use of such a mirror enables highly dynamic focus correction on a large working plane.

2. Optomechanical setup and working principle

The active mirror is implemented in the optical system as a 90° deflecting mirror. A focal lens is implemented in the beam path between active mirror and X-Y-scanner and focuses the beam on the work plane. Figure 1 shows the working principle of the plane field correction concept by use of an active mirror. By deforming the surface of the active mirror, the optical power is changed so that the initially collimated beam diverges. This increases the resulting focal length of the lens - active mirror system and the focus position can be shifted

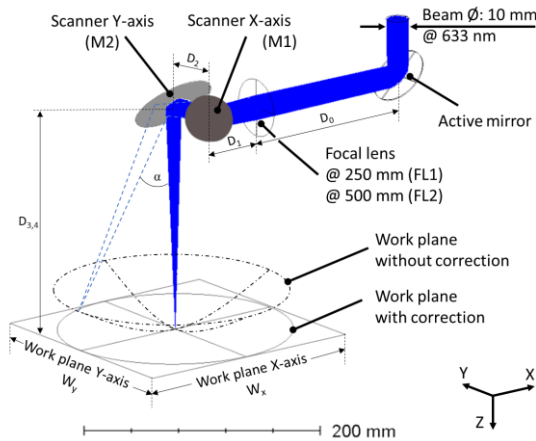


Fig. 2. Working principle of the plane field correction by use of an active

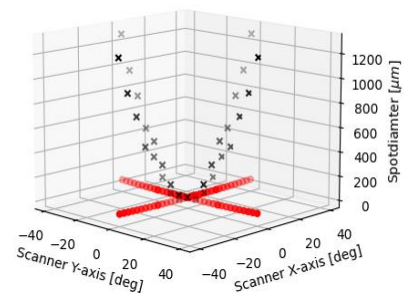


Fig. 1. Spot diameter in relation to the scan angles X and Y. Without activation of the active mirror (black cross). With activation of the active mirror (red dots)

along the beam direction. A change in the scanner deflection causes an elliptical distortion in the edge areas of the X-Y-work plane. Depending on the optical power of the active mirror, the focus position can be adjusted and the distortions in the peripheral areas can be minimized. Figure 2 shows the effect of focus tracking for a lens focal length of 250 mm. It can be clearly seen that as the optical scan angle changes (black crosses), the spot size increases. The use of an active mirror corrects the spot for the entire scan range (red dots).

3. Design of the active mirror

The active mirror design is based on an unimorph concept using a piezoelectric disc bonded to a thin glass substrate with a highly reflective multilayer coating. Thus, standard glass polishing, and coating technologies may be used for mirror finishing. Figure 3(a) shows a picture of the Zwobbel[®]-1020 that has been used for the experimental verification (RobustAO, 2021). The elliptical aperture is optimized for 90° laser beam deflection. The flange front surface is used to fix the active mirror via four screws and the two small bores are used for pin alignment. Optical tests are used to verify the optical surface and vibrometric measurements verify the temporal behaviour.

Figure 3(b) shows a characteristic measurement of the step response of the uncontrolled mirror

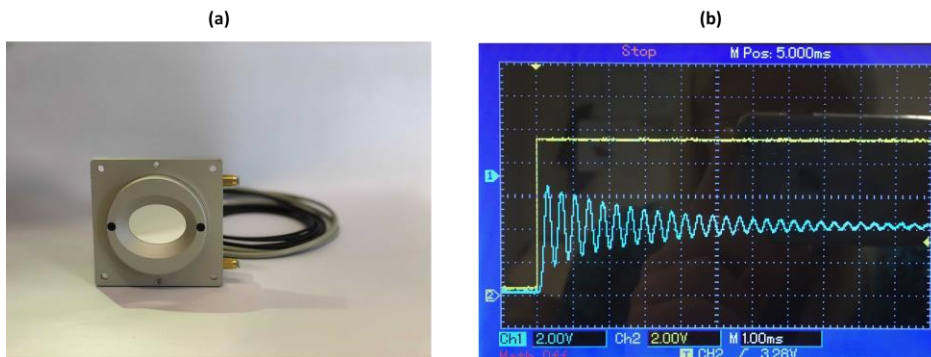


Fig. 3. Picture of the Zwobbel[®]-1020 that has been used in that experiments (a). Measured step response of the Zwobbel[®] to calculate the resonance frequency to 2.6 kHz (b).

surface. The stepwise activation initiates the mirror deflection that is superimposed by a sinusoidal oscillation reflecting the resonance frequency of the system $f_R = 2.6$ kHz. That frequency is in good agreement with the simulated resonance frequency of 2.8 kHz. Using the measured resonance frequency, the response time $t_{SR} = (= 1/(3f_R)) = 133\mu s$ for the full stroke is calculated. Together with the controller and active mirror voltage supply, a minimal controlled full stroke step response of two milliseconds is achieved.

In flat field scanning system, the required z-position is minimal in the centre of the field and maximal at the corners. Thus, the real scanning time depends on the scan pattern, but as state-of-the-art z-scan systems offer full stroke step responses between 4 milliseconds and 200 milliseconds depending on the activation technology, the Zwobbel[®] technology will speed up z-scan applications.

4. Methods of evaluation

To evaluate active mirrors in plan field correction, we developed the measurement setup as shown in Figure 1 that is set up in ZEMAX OpticStudio and as evaluation experiment. For the best comparability between the optic simulation and the measurement setup the same parameters (Table 2) were used for both.

In the optic simulation, a defined optical scan angle (α) and the radii of curvature of the active mirror defined as variables can be used to determine the minimum spot size as a function of the scan angle. To describe the spot, the Huygens PSF was evaluated in a defined work plane. As a criterion for the spot size, the Gaussian beam radius was used, which is characterized with $1/e^2$ decrease of the beam intensity. To determine the simulated spot diameters, the spot image a pixel size of $1.4 \mu\text{m}$ was taken. In the experimental measurements, the image of the spot was taken with a camera with a pixel size of $3.2 \mu\text{m}$. These measurements were repeated for different scan angles and the voltage-dependent deformation of the active mirror is adapted in regard of the minimum spot diameter.

In addition, the eccentricity (Figure 4) is considered to evaluate the spot quality in simulation and experiment. The eccentricity ε is a characteristic that describes the deviation from the circular shape.

$$\varepsilon = \frac{\sqrt{a^2 - b^2}}{a} \quad (1)$$

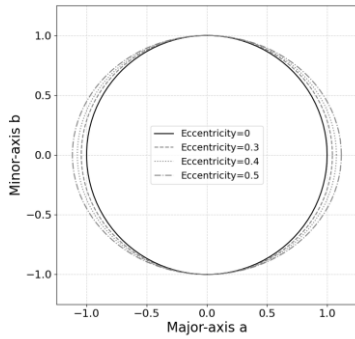


Fig. 4. Eccentricity ε of the laser spot

Table 1. Spot eccentricity and ratio of major- to minor axis.

Eccentricity ε	Ratio a/b [%]
0	0
0.3	5
0.4	10
0.5	15

Accordingly, an eccentricity of 0 is a circle. An eccentricity of 0.3 describes a deviation from the major axis to the minor axis of 5%. With an eccentricity of 0.4 this deviation is 10% and 15% at an eccentricity of 0.5 (see table 1). By knowing the distance between the scan mirror and the working plane, the dimensions of the work plane W_x and W_y can be calculated.

$$W_x = \tan(\alpha) \cdot (D_2 + D_{3,4}) \quad (2)$$

$$W_y = \tan(\alpha) \cdot D_{3,4} \quad (3)$$

Table 2. Parameters of the optic simulation and the measurement setup

Parameter	Symbol	Value
Wavelength	λ	633 nm
Collimated beam diameter	\varnothing	10 mm
Beam quality	M^2	1
Deflection angle of the active mirror		90°

Distances:		
Active mirror – focal lens	D_0	250 mm
Focal lens – Scan mirror X-axis	D_1	50 mm
Scan mirror X-axis – Scan mirror Y-axis	D_2	50 mm
Scan mirror Y-axis – Working plane @ $f=250$ mm	D_3	150 mm
Scan mirror Y-axis – Working plane @ $f=500$ mm	D_4	400 mm

5. Discussion and results

5.1. Simulated performance of requirements of the active mirror

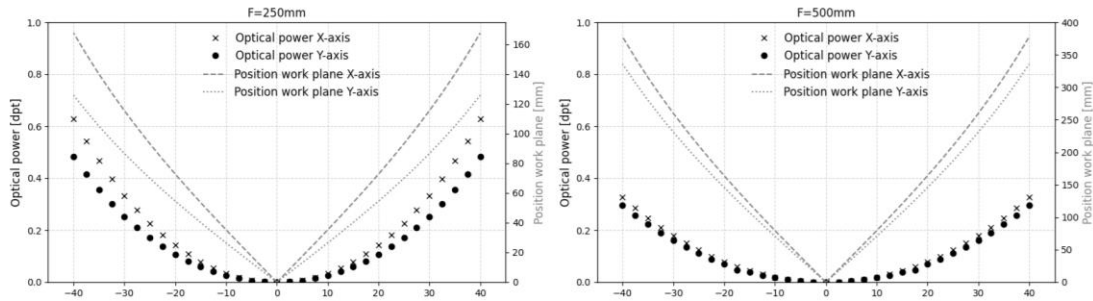


Fig. 5. Optical power of the active mirror for a focal length of 250 mm (left) and 500 mm (right) in relation to the scan angle.

To correct the spot distortion due to increasing scan angles, the nominal focus position must be shifted. The nominal focal length is given by the focal length of the focus lens. By increasing the optical scan angle, the active mirror must assume smaller radii of curvature R_x and R_y to generate the smallest spot on the work plane. These quantities can be measured by a Zernike description of the active mirror using a wavefront sensor (Böttner, P., et al). The optical power D is the reciprocal value of the radii of curvature of the active mirror. By changing the optical power D of the active mirror, the focus of the active mirror-lens system is shifted. To compensate the astigmatic distortion of the wavefront due to the 90° mounting position of the active mirror the mirror must have a biconically formable surface. This surface is described by different radii of curvature in X and Y direction. The further the focus of the active mirror lens system is to be shifted, the smaller the radius of curvature of the active mirror must be. Due to the fixed ratio of the radii of curvature, the optical power D of the mirror is determined via the reciprocal value of the radius of curvature of the X-axis (R_x).

$$D = \frac{1}{R_x} \quad (4)$$

Figure 5 shows the simulation results of the relationship between the optical power and the optical scan angle. The maximum optical power is 0.63 dpt for a focus lens with 250 mm and 0.3 dpt for a focus lens with 500 mm and an optic scan deflection of $\pm 40^\circ$. The curves are parabolic and symmetrical with the Y-axis. Due to the different distances between the two scan mirrors and the working plane, the result is an asymmetrical work plane. For a focal length of 250 mm, the working range of the X-axis is 25% larger than that of the Y-axis, with a maximum optical angle of $\pm 40^\circ$. When using a focal length of 500 mm, the difference between the X- and Y-axis is 11%. This results in an elliptical working field with the dimensions (333 x 250) mm² when using a focal length of 250 mm and (755 x 670) mm² when using a focal length of 500 mm.

5.2. Performance of the active mirror

Figure 6 shows the Zernike decomposition of the Zernike coefficients from C3 to C13 for different optical powers of the active mirror. The dominant Zernike coefficients of defocus (C3) and astigmatism (C4) are clearly visible. The mirror already has an initial deformation which is evident in an optical power of 0.4 dpt. The optical power at maximum mirror deformation is 0.92 dpt. This leaves an optical power range of 0.52 dpt. The measured Zernike coefficients are transferred to the simulation model to describe the surface.

The RMS_{error} of the wavefront can be determined as a quantity of the shape accuracy as the deviation of the measured surface from an ideal biconical surface. Figure 7 shows a linear increase of the RMS_{error} from

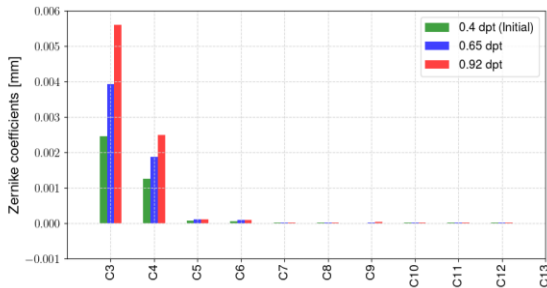


Fig. 6. Zernike coefficients for different optical powers.

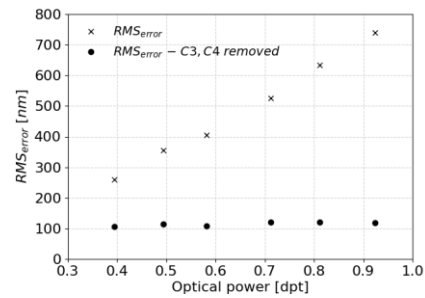


Fig. 7. Surface shape errors (RMS_{error}) in relation to the optical power of the active mirror. Absolute RMS_{error} (Black crosses). RMS_{error} Zernike coefficients C3 and C4 removed (Black dots).

259 nm at 0.4 dpt to 739 nm at 0.92 dpt. Subtracting the Zernike coefficients C3 and C4 results in a constant RMS_{error} of 110 nm over the entire optical power range.

To evaluate the dynamics of the active mirror, the step response time of 2 milliseconds was used. Knowing the size of the working plane, the working speed of the mirror can be calculated.

Focal length	Work plan $W_{x,y}$ [mm]	Working speed $v_{x,y}$ [m/s]
250 mm	X	83.25
	Y	62.5
500 mm	X	188.75
	Y	167.5

shows the working speed in relation to the focal length and the dimensions of the working plane (see figure 5).

$$v_{x,y} = \frac{W_{x,y}}{t_{SR}} \quad (5)$$

Table 3. Working speed of the active mirror in relation to the focal length and the dimensions of the work plane.

Focal length	Work plan $W_{x,y}$ [mm]	Working speed $v_{x,y}$ [m/s]
250 mm	X	83.25
	Y	62.5
500 mm	X	188.75
	Y	167.5

5.3. Plane field correction for $f=250$ mm

To evaluate the plane field correction for a fixed lens focal length of 250 mm, a comparison is carried out between simulation and measurement setup. The geometric dimensions are shown in Table 1 and are identical for simulation and measurement.

In the reference position of the scanner mirrors, the beam is incident perpendicular to the working plane. The simulated spot diameter is $29.5 \mu\text{m}$ in this position. An elliptic distortion of the spot occurs with increasing optical scan angle and thus an increasing work plane. To describe this eccentricity, the spot is described by its major- and minor-axis. The limit of eccentricity is defined as 0.3, 0.4 and 0.5 (see Figure 4). Figure 8 shows the

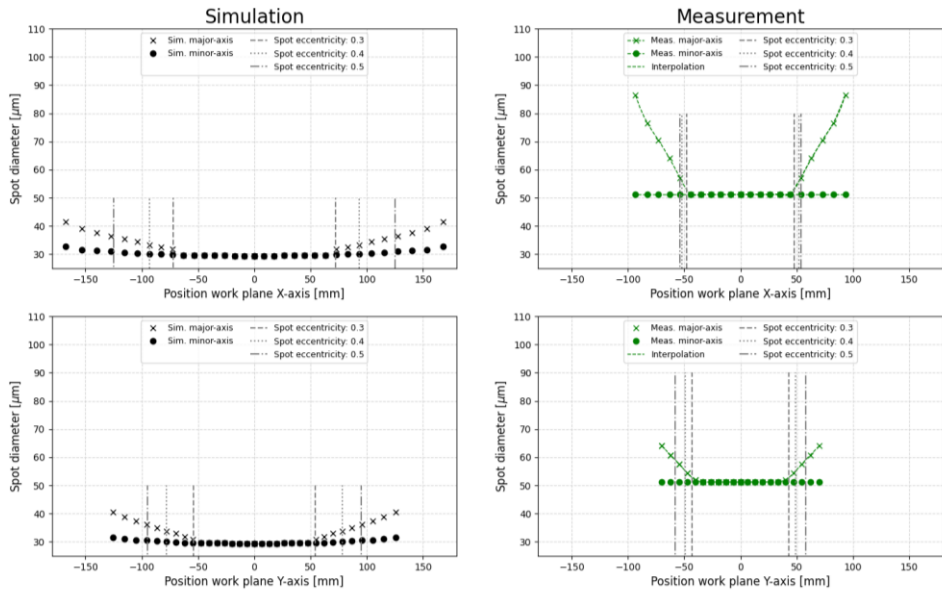


Fig. 8. Major- and minor-axis of the spot in relation to the work plane X-axis (left) and Y-Axis (right). Simulated (black) and measured spot (green).

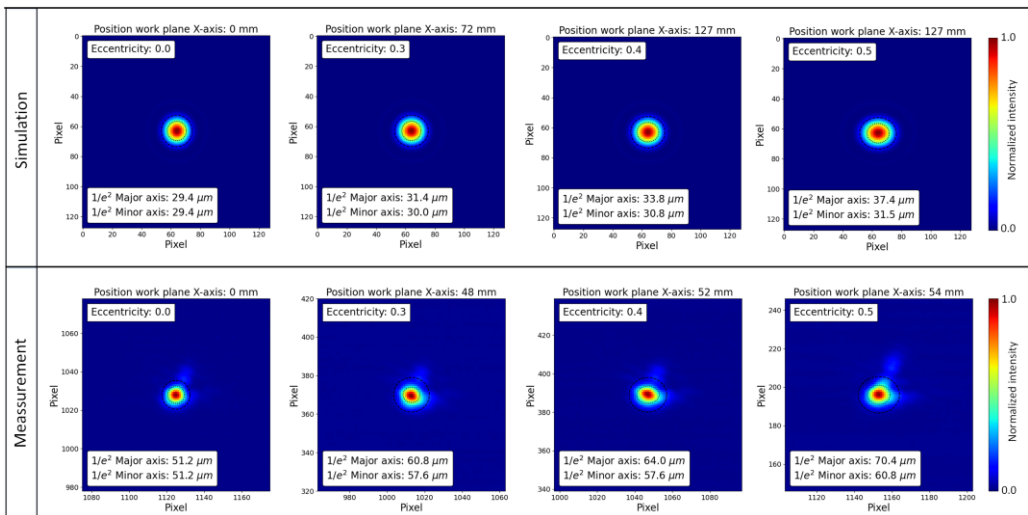


Fig. 9. Spot at the work plane X-axis for simulation (top) and measurement (bottom) for a focal length of 250 mm.

spot diameters of the major-axis and minor-axis of the spot as a function of the spot position on the X-Y-work plane. The optics simulation shows that a work field of (128x110) mm² is achieved with an eccentricity of up to 0.3. An eccentricity of 0.4 enables a work field of (186x140) mm² and an eccentricity of 0.5 enables a work field of (250x190) mm².

F-Theta optics with a comparable focal length (f=255 mm) allow a work plane of (114x114) mm² (Jenoptik AG). The simulations show that this working field is also possible with an active mirror and a permissible eccentricity of 0.3. If an eccentricity of 0.4 is allowed, the working field increases by 32% and with an eccentricity of 0.5 by 54% in the X-direction of the working plane. In the Y-direction, an enlargement of the working plane of 21% can be achieved with an eccentricity of 0.4 and 42% with an eccentricity of 0.5. The results of the simulation can be confirmed quantitatively by measurements. The measured spot diameter in the reference position is 51.2 μm and thus significantly larger than in the optics simulation. The work plane is (96x96) mm² with a spot eccentricity of 0.3 and increases to (110x120) mm² with an eccentricity of 0.5. Figure 9 shows an example of the X-axis spot images for different spot eccentricities at different points on the work plane.

The differences between the measured and simulated spot diameters are due to the surface shape errors of the active mirror. These errors of the active mirror lead to an enlargement of the spot diameter and a reduction of the working field in the measurements.

5.4. Plane field correction for f=500 mm

The simulation of the plane field correction with a focal length of 500 mm results in a minimum spot diameter in the reference position of 57.4 μm. Figure 10 shows the simulated spot diameter for the X- and Y-axis of the work plane. The simulated minor-axis increases to 59.1 μm with a spot eccentricity of 0.3, to 61.1

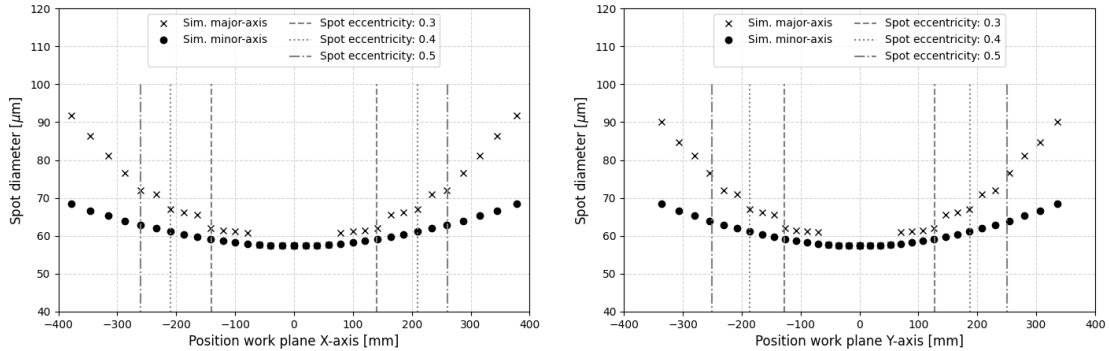


Fig. 10. Major- and minor axes of the spot in relation to the work plane X-axis (left) and Y-Axis (right). Simulated (black)

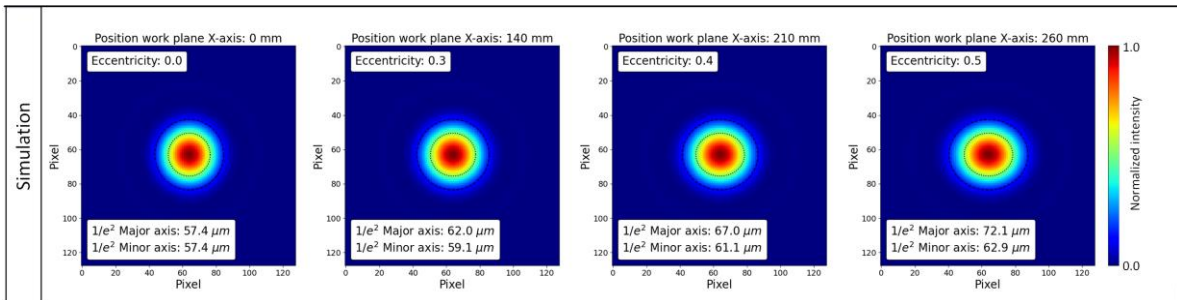


Fig. 11. Spot at the work plane X-axis for a simulated focal length of 500 mm.

μm with an eccentricity of 0.4 and to $62.9 \mu\text{m}$ with an eccentricity of 0.5. The associated working plane extends to $(282 \times 252) \text{ mm}^2$ with a spot eccentricity of 0.3, to $(420 \times 372) \text{ mm}^2$ with an eccentricity of 0.4 and to $(520 \times 460) \text{ mm}^2$ with an eccentricity of 0.5. Figure 11 shows the spot image of different spot eccentricities and their position on the work plane.

Compared to an F-Theta lens with a focal length of 510 mm and a field size of $(328 \times 328) \text{ mm}^2$ (Jenoptik AG, 2021), the use of an active mirror allows a comparable field size with a spot eccentricity between 0.3 and 0.4.

From that, we conclude that compared to F-Theta applications, similar work fields are enabled. Moreover, just a fraction of the actuation range of the Zwobbel[®] is used for the pure plan field correction. The remaining actuation range may be used for 3D-volumes.

5.5. Active mirror induced 3D-work volume

In this section, the relationship between spot eccentricity and optical power will be investigated based on the ideal active mirror. The actuation range of the ideal active mirror at a lens focal length $f = 250 \text{ mm}$ is larger than needed for plane field correction. Thus, the working field may be shifted. Figure 12 shows the relationship of both spot eccentricity and optical power as a function of the spot position in the X-Y-work plane. As already known, the eccentricity increases with increasing distance from the reference position. Considering the spot eccentricities of 0.0, the optical power required for achieving this is $\sim 0.1 \text{ dpt}$. Therefore, the active mirror must have a high sensitivity and adjustment accuracy at low optical powers (up to 0.1 dpt) to generate a small spot in the work plane. However, the active mirror has an optical power range of 0.52 dpt . This makes it possible to shift the entire working plane in the Z-direction with optical power greater than 0.1 dpt and thus create a

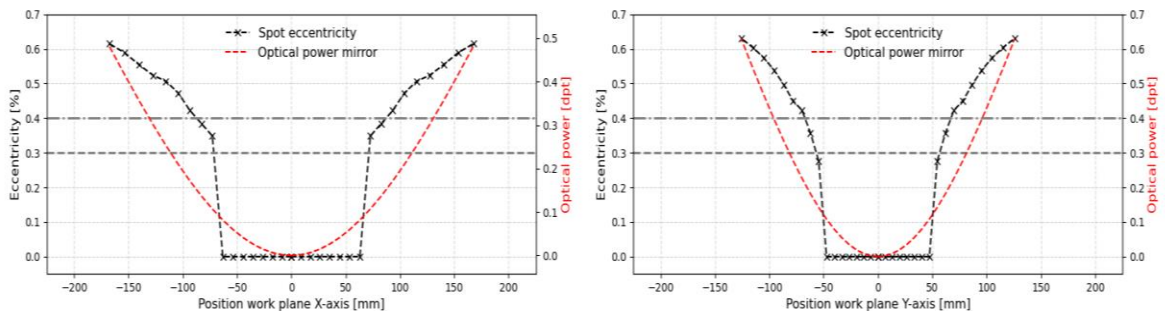


Fig. 12. Spot eccentricity and optical power in relation to the work plane axis. X-axis (left). Y-axis (right).

3D-work volume. Thus, an optical power of $\sim 0.1 \text{ dpt}$ is used for plan field correction of a work field of $(110 \times 100) \text{ mm}^2$. The remaining 0.42 dpt enable a 3D-work volume of $(110 \times 100 \times 31) \text{ mm}^3$. The plane field correction system may be tailored to applications, larger fields are possible at the cost of smaller z-height.

6. Conclusion and Outlook

The results show that the use of an active mirror enables highly dynamic plane field correction. Simulations of an ideal active mirror result in an X-Y working field size of $(186 \times 140) \text{ mm}^2$ with a fixed lens focal length of 250 mm and a maximum spot eccentricity of 0.4. The minimum spot diameter for this configuration is $29.5 \mu\text{m}$. Compared to an f-theta lens of a post-objective scanning solution with a focal length of 255 mm, the active mirror enables a work plane that is up to 32% larger. The simulation with a doubling of the lens focal length to 500 mm allows an X-Y working field of $(420 \times 372) \text{ mm}^2$ with an eccentricity of 0.4.

Thus, active mirrors for plane field correction are adventurous for focal length larger 250 mm compared to F-Theta applications and in particular for 3D-applications. In a measurement setup, the results of the simulation were quantitatively confirmed with a focal length of 250 mm. Due to the surface shape errors and the shape deviation of the active mirror, the diameter of the measured spot is 51.2 μm . In addition, the usable X-Y working plane is reduced to (96x96) mm^2 .

The measured step response time of 2 ms allows a highly dynamic spot correction in the X-Y work plane ((100x100) mm^2) of 25 m/s. An active mirror in combination with a focal lens ($f=250$ mm) must allow a change in optical power of 0.1 dpt to correct a work plane of 110 x 110 mm. Remaining optical power may be used for substantial 3D-volumes. The remaining 0.42 dpt of the Zwobbel[®] mirror would enable a 3D-work volume of (110 x100x31) mm^3 . Considering that the z-scan speeds exceed 25 m/s the speeds of typical X-Y-scanners, true 3D machining at high speeds in all three axes is possible through the Zwobbel[®].

The theoretical considerations on the size of the working volume as well as the influence on the dynamic behaviour of the entire system are part of further investigations.

Acknowledgements

The authors are grateful for the financial support within the project: "Digital Innovation Hub Photonics (DIHP)"

References

- A. R. Bayanna, R. E. Louis, S. Chatterjee, S. K. Mathew, and P. Venkatakrishnan, "Membrane-based deformable Böttner, P., et al. "Design routine and characterisation of a biconic deformable metal mirror for focus shifting." *Optics Express* 29.3 (2021): 2971-2983.
- Eberle, Gregory, Vincent Chiron, and Konrad Wegener. "Simulation and realization of a focus shifting unit using a tunable lens for 3D laser material processing." *Physics procedia* 41 (2013): 441-447.
- Jenoptik AG, 2021 <https://www.jenoptik.de/produkte/optische-systeme/objektive-lasermaterialbearbeitung/silverline-f-theta> (Bestellnummer: 017700-026-26 updatet: 19.05.2021)
- Jenoptik AG, 2021 <https://www.jenoptik.de/produkte/optische-systeme/objektive-lasermaterialbearbeitung/f-theta-selektor> (Bestellnummer: 017700-405-26 updatet: 19.05.2021)
- Kopf, Teresa, et al. "Adapting the axial focus in high-power laser processing machines within mm-range." *High-Power Laser Materials Processing: Applications, Diagnostics, and Systems VI*. Vol. 10097. International Society for Optics and Photonics, 2017. mirror: intrinsic aberrations and alignment issues," *Appl. Opt.* 54(7), 1727–1736 (2015).
- Pelsue, Kurt. "Precision, post-objective, two-axis, galvanometer scanning." *High Speed Read/Write Techniques for Advanced Printing and Data Handling*. Vol. 390. International Society for Optics and Photonics, 1982.
- Reinlein, Burkhardt, Gier: „Zwobbel[®]-driven high speed focussing in laser machining.“ Proc. 12. Jenaer Lasertagung 14.-15. 2021, Jena, Deutschland
- Reinlein, Claudia, et al. "Performance of a thermal-piezoelectric deformable mirror under 6.2 kW continuous-wave operation." *Applied optics* 52.34 (2013): 8363-8368.
- RobustAO GmbH, 2021 <https://robustao.de/zwobbel-fast-focussing-solution/technical-specifications-zwobbel-1020/> updatet: 19.05.2021)
- S. Verpoort, M. Bittner, and U. Wittrock, "Fast focus-shifter based on a unimorph deformable mirror," *Appl. Opt.* 59(23), 6959–6965 (2020).
- Wood, Roger M. *Laser-induced damage of optical materials*. CRC Press, 2003.
- Zaeh, M. F., et al. "Material processing with remote technology revolution or evolution?." *Physics Procedia* 5 (2010): 19-33.